MDPI

Article

Influence of Liquid Hydrogen Diffusion on Nonlinear Mixed Convective Circulation around a Yawed Cylinder

Prabhugouda M. Patil [1,2], Hadapad F. Shankar [1] and Mikhail A. Sheremet [3,*]

1 Department of Mathematics, Karnatak University, Pavate Nagar, Dharwad 580003, India; pmpmath@gmail.com (P.M.P.); shankarhf@gmail.com (H.F.S.)
2 Pavate Institute of Mathematical Sciences (PIMSci.), Karnatak University, Pavate Nagar, Dharwad 580003, India
3 Laboratory on Convective Heat and Mass Transfer, Tomsk State University, 634050 Tomsk, Russia
* Correspondence: sheremet@math.tsu.ru; Tel.: +7-3822-529740

Abstract: A yawed cylinder is a cylinder inclined in the plane of a flowing liquid. The liquid flow past the yawed cylinder is important for practice, namely, for bubble suppression and control of the boundary layer transition in undersea applications. It should be noted that an inclined cylinder characterizes an asymmetrical behavior of fluid flow and heat transfer. Energy and mass transference characteristics of a steady nonlinear convective flow over the yawed cylinder by accounting for chemically reactive species and viscous dissipation are analyzed in this investigation. The differential equations defining the boundary layer parameters are then transformed into a dimensionless view, taking into account the non-similar transformation. It should be noted that the governing equations have been written using the conservation laws of mass, momentum, energy, and concentration. These considered equations allow the simulation of the analyzed phenomenon using numerical techniques. Further, quasilinearization and implicit finite difference approximation are used to work out the non-dimensional governing equations. A parametric investigation of all the pertinent characteristics accompanies this. A descriptive system of computation outcomes for the velocity, temperature, and concentration patterns, the drag coefficients, Nu and Sh, is demonstrated by graphs. Enhancing the magnitudes of the Eckert number raises the temperature pattern while energy transport strength is reduced. As the species concentration profile diminishes, the mass transfer characteristics are enhanced for raising magnitudes of the nonlinear chemical reaction parameter. Further, a velocity profile along the chordwise direction rises with enhancing magnitudes of nonlinear convection characteristics and yaw angle. Furthermore, the velocity pattern along the spanwise direction enhances with the growing magnitudes of yaw angle. For assisting buoyancy flow, the friction parameter at the border in the spanwise direction enhances with rising values of yaw angle.

Keywords: mixed convection; yawed cylinder; viscous dissipation; nonlinear chemical reaction; nonlinear convection parameter; quasilinearization technique

1. Introduction

Due to the enhanced engineering and industrial applications, researchers have studied a broad spectrum of boundary layer motion challenges. Particularly, the motion along a yawed cylinder is studied due to its various engineering applications, such as tow cables, braced frame members, suspension of bridges, overhead cables, and raked marine files, etc. [1,2]. Chiu and Leinhard [3] have analyzed the fluid motion around a yawed cylinder. Their outcomes exhibit that the separation position will occur beyond the crosswise direction and is free from a yaw angle in a spanwise direction. Further, King [2] has reported oscillations of the yawed cylinder and analyzed that the cylinder reacts almost identically for positive as well as negative yaw angles. Moreover, Bucker and Lueptow [4] have analyzed the border layer on a weakly inclined cylinder, and the obtained outcomes

exhibit that as the yaw angle varies, nonlinearly the thickness of the border layer varies. Different studies [5–7] show the effect of single slot injection (suction) into steady water and compressible boundary layer flows over two-dimensional and axi-symmetric bodies. Subhashini et al. [5] have analyzed the motion around a yawed circular cylinder with multiple injections, yielding results that the non-uniform multiple slot suction postpones the separation location. Roy [6] studied the mass transfer over the yawed cylinder, demonstrating that the non-uniform suction postponed the separation. Later, Roy and Saikrishnan [7] analyzed the slot injection over the yawed cylinder showing that, as the viscous dissipation parameter enhances, the Nusselt number diminishes. Further, Saikrishnan [8] has reported the boundary layer circulation around the yawed cylinder, and his study exhibits the extended separation position by the non-uniform multiple slot suction. Moreover, Revathi et al. [1] have worked on unsteady motion along with the yawed cylinder by considering the effects of non-uniform mass transfer, revealing the reduction of velocity border layer size in the *x*-direction, while there is an increase in *z*-direction due to the presence of unsteadiness in the fluid flow. Marshall [9] has analyzed the yawed cylinder in wake dynamics (disturbed flow). His outcomes exhibit that the axial boundary layer is detected thin and thick in the upstream and downstream sides of the cylinder, respectively. Further, Najafi et al. [10] have observed the yawed cylinder in a disturbing motion under the time dependence and have observed two different flow patterns for the variation of yaw angle. Wang et al. [11] have examined the impact of yaw angle above a circular cylinder, and it has been observed that the shear layers are stronger as the angle enhances. Liang and Duan [12] have reported the motion along with the inclined cylinder with the influence of lateral end surfaces, and the results show that the separation point shifts upwards with the enhancement in the yaw angle. Sears [13] has examined the border layer motion in a yawed cylinder. Snarski [14] has reported the examination of flow along with an inclined cylinder and shown that *Re* effects are prominent at small yaw angles. Zhao et al. [15] have examined 3D motion along with a yawed circular cylinder. Moreover, Thapa et al. [16] have analyzed numerically the fluid motion over an inclined cylinder close to the plane border. In the work of Gupta and Sarma [17], the time-dependent circulation along an inclined infinite cylinder under the effect of cross-flow has been analyzed, showing that the coefficient of friction along the chordwise direction diminishes with larger values of the non-similar variable (ζ). Recently, Jenifer et al. [18] have worked on steady MHD flow over a yawed cylinder with mass transfer, and their results reveal that the separation can be slowed down by enhancing the MHD parameter. Khan et al. [19] have worked on hybrid nanofluid flow over a yawed cylinder, and their results reveal that the yaw angle enhances the velocity in the spanwise and chordwise directions, whereas the temperature declines.

In many industrial processes occurring in material manufacturing, the difference between the ambient temperature and that of the wall need not be small, and the significant difference in these temperatures causes a remarkable impact on the heat transfer and fluid flow characteristics that determine the quality of the manufactured material sheet or fiber. In such cases, the assumption of linear density temperature variations in the buoyancy force term presented in the governing equations of the flow may yield inaccurate results. In order to achieve comprehensive results in such situations, one needs to study nonlinear convection. Therefore, we aim to account for the nonlinear density temperature (NDT) variations in the buoyancy force term in the present analysis. Very few researchers have studied nonlinear convection; to name a few are Vajravelu and Sastri [20], Bhargava and Agarwal [21], Mandal and Mukhopadhyay [22], and Khan et al. [23]. Some interesting results can be found also in [24–27].

Combined convection flows appear when the temperature and species concentration variations between environmental liquid and the yawed cylinder shell are larger. Hence, it becomes important when buoyancy forces significantly disturb the velocity, temperature, and concentration patterns. Double-diffusive convection occurs when the liquid is confined to two distinct density gradients with different diffusion coefficients. The gradients can influence the change in density in the liquid concentration or the temperature variations.

The double-diffusive combined convection flow has an essential value in border layer flow problems owing to its significance in numerous technical and geophysical challenges, solar collectors, solar ponds, lakes, reservoirs, and crystal growth, to mention a few [28]. Many researchers have worked on double-diffusive combined convection flows [29,30]. In the work of Grosan and Pop [31], a combined convection flow over a vertical cylinder has been analyzed, revealing the reduction in the velocity border layer whilst the temperature border layer enhances with the nanoparticle volume fraction. Recently, Prasannakumara et al. [32] reported a double-diffusive boundary layer flow around the stretching sheet showing a decline in velocity for growing magnitudes of Maxwell characteristics. Abdal et al. [33] have worked on the thermo-diffusion effect on MHD unsteady mixed convection of micropolar fluid over a stretching/shrinking sheet. Their results reveal that the fluid velocity, temperature, solutal, and nanoparticle profiles are seen to increase with an increment in the unsteadiness parameter. Lund et al. [34] have worked on the convective impact of magnetohydrodynamics Casson fluid over a vertical exponential stretching/shrinking surface. Their result reveals that the fluid temperature reduces in all solutions and both surfaces when the effect of *Pr* increases. Patil et al. [35] have worked on mixed convection hybrid nanofluid flow over a sphere. Their results reveal that the surface drag coefficient and energy transport strength are enhanced for rising values of combined convection characteristics. Muthukumaran and Bathrinathan [36] have worked on mixed convection flow over a stretching sheet in the presence of viscous dissipation. Their results reveal that the heat transfer rate increases with the increase in *Pr* for both assisting and opposing flows. Zaib et al. [37] have worked on mixed convection flow over a Riga surface. Khan et al. [38] have worked on mixed convection hybrid nanofluid flow through a vertical stretching/shrinking wedge. Hsiao [39] has worked on combined convection Carreau nanofluid flow over a stretching sheet. Patil et al. [40–42] have studied the double-diffusive convective motion past different geometries, such as an exponentially stretching surface, sphere, etc.

Chemical reaction impacts on energy and mass transference have a significant value in hydrometallurgy and chemical technologies [43,44]. Malarselvi et al. [45] have worked on the influence of chemical reaction on MHD double-diffusive flow, yielding results that the chemically reactive characteristics diminish the concentration with/without suction/injection. Patil et al. [46,47] have worked on a boundary layer circulation past the surface under the chemical reaction effects. Recently, Hayat et al. [48] worked on the non-linear convective motion past the stretching cylinder under a chemical reaction influence, revealing that the concentration reduces for a destructive chemical reaction. In the work of Reddy and Chamkha [49], the investigation of natural convection over a vertical cone under the chemical reaction influence has been analyzed.

However, the mixed convection influence plays a prominent role in determining the boundary layer parameters of motion over a yawed cylinder. From the above studies of literature, it has been observed that the examination of double-diffusive nonlinear convection flow past a yawed cylinder under the influences of viscous dissipation and nonlinear chemical reaction effects have not been attempted so far. Therefore, many authors such as Roy [6], Chiu and Lienhard [3], Roy and Saikrishnan [7], and Revathi et al. [1] have studied a forced convection boundary layer circulation past the yawed cylinder. These studies' vast areas of applications include many engineering and industrial fields, including subsea pipelines, towers, offshore structures, chimney stacks, risers, etc. [1]. Studies of these authors have motivated us to work on the current study. It has been observed that much attention has not been paid to mixed convection circulation over an inclined cylinder. Therefore, we are interested in studying mixed convective motion past the yawed cylinder under the effects of viscous dissipation and chemically reactive species with the novelty of the work as follows:

- Combined convection flow past a yawed cylinder;
- Influence of nonlinear chemical reaction over the yawed cylinder;
- Impact of nonlinear convection over the yawed cylinder;

-      Influence of liquid hydrogen diffusion due to the yawed cylinder.

The formulated governing equations with border constraints have been investigated using suitable non-similar reduction, and theoretical analysis has been performed employing the method of quasilinearization and implicit finite difference approximation [6,7].

2. Mathematical Simulation

A steady laminar incompressible liquid motion past a yawed cylinder is assumed for investigation. Let R be the cylinder's radius, C_w and T_w are concentration and temperature at the wall, and C_∞ and T_∞ are concentration and temperature away from the wall, respectively. The flow system with physical parameters is displayed in Figure 1. It should be noted that an inclined cylinder characterizes an asymmetrical behavior of fluid flow and heat transfer. Here, the value $\theta = 0$ indicates the vertical cylinder, while $\theta = \pi/2$ indicates the horizontal cylinder. Thus, in order to have the effects of the yawed cylinder, we have considered the value of the yaw angle θ in between 0 and $\pi/3$. Since the problem is of mixed convection, the cylinder needs to be considered in a vertical or inclined position to have the buoyancy effects. Moreover, the values of θ above $\pi/3$ are not considered since they would be closer to stagnation point flow, and it is not the objective of the present mixed convection flow analysis. Here, x is the curvilinear coordinate in the chordwise direction with u being its velocity, while coordinate y is in the normal direction with v being its corresponding velocity; z is the coordinate in the spanwise direction with w being its corresponding velocity component and θ is the yaw angle. The subscript w refers to the condition at the surface, ∞ refers to the condition in the main flow, and e being the condition at the boundary layer edge. The density changes are modelled through the Boussinesq approach [50].
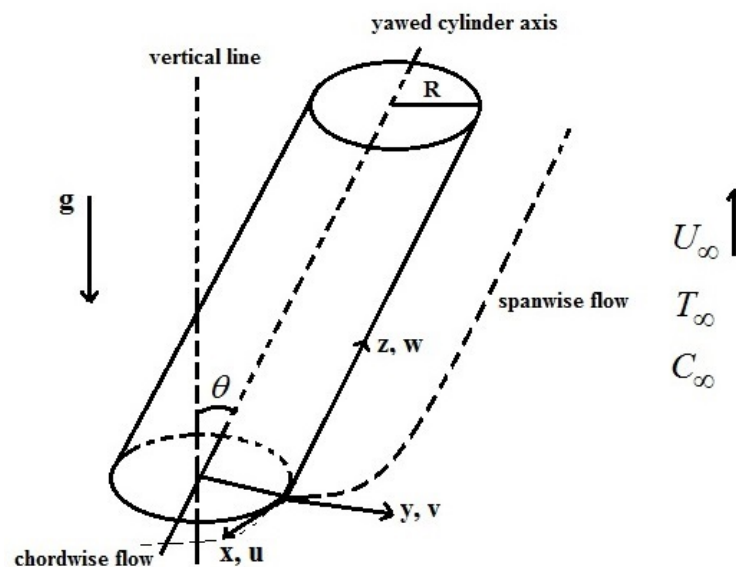

Figure 1. Physical view of the circulation and coordinate system.

The temperature of the yawed cylinder border is T_w, where $T_w > T_\infty$ for aiding buoyancy motion and $T_w < T_\infty$ for opposing buoyancy motion. This problem is formulated with the non-similar approach. The outcomes attained in this study approve that the FDM is a powerful mathematical tool, and it can be used in a large class of linear and nonlinear problems arising in several fields of science and engineering. For more simplification of the given model, the following assumptions are employed:

- Steady flow
- Incompressible flow
- Mixed convection flow (assisting and opposing flows)
- Yawed cylinder

- Boundary layer approximations
- Boussinesq approximation

Taking into account these mentioned assumptions, the border layer relations and corresponding boundary constraints are [5–8,51–53]:

$$\frac{\partial u}{\partial x} + \frac{\partial v}{\partial y} = 0 \tag{1}$$

$$
\begin{aligned}
u\frac{\partial u}{\partial x} + v\frac{\partial u}{\partial y} = u_e\frac{du_e}{dx} + g\left\{\beta_1(T-T_\infty) + \beta_2(T-T_\infty)^2 + \ldots\right\}\sin(\theta) \\
+ v\frac{\partial^2 u}{\partial y^2} + g\left\{\beta_3(C-C_\infty) + \beta_4(C-C_\infty)^2 + \ldots\right\}\sin(\theta)
\end{aligned}
\tag{2}
$$

$$
\begin{aligned}
u\frac{\partial w}{\partial x} + v\frac{\partial w}{\partial y} = v\frac{\partial^2 w}{\partial y^2} + g\left\{\beta_1(T-T_\infty) + \beta_2(T-T_\infty)^2 + \ldots\right\}\cos(\theta) \\
+ g\left\{\beta_3(C-C_\infty) + \beta_4(C-C_\infty)^2 + \ldots\right\}\cos(\theta)
\end{aligned}
\tag{3}
$$

$$u\frac{\partial T}{\partial x} + v\frac{\partial T}{\partial y} = \frac{k}{\rho c_p}\frac{\partial^2 T}{\partial y^2} + \frac{v}{c_p}\left(\left(\frac{\partial u}{\partial y}\right)^2 + \left(\frac{\partial w}{\partial y}\right)^2\right) \tag{4}$$

$$u\frac{\partial C}{\partial x} + v\frac{\partial C}{\partial y} = D_B\frac{\partial^2 C}{\partial y^2} - k_1(C-C_\infty)^n \tag{5}$$

$$
\left.
\begin{aligned}
y = 0: \quad & u = 0,\ v = 0,\ w = 0,\ C = C_w,\ T = T_w, \\
y \to \infty: \quad & u \to u_e(x) = 2u_\infty\sin\left(\tfrac{x}{R}\right),\ w \to w_e = w_\infty\cos\theta,\ C \to C_\infty,\ T \to T_\infty
\end{aligned}
\right\} \tag{6}
$$

The non-similar transformations are as follows [6,7]:

$$
\left.
\begin{aligned}
& \xi = \int_0^x \frac{u_e}{u_\infty}d\left(\tfrac{x}{R}\right), \qquad \eta = \left(\frac{Re}{2\xi}\right)^{\frac{1}{2}}\left(\frac{u_e}{u_\infty}\right)\frac{y}{R}, \\
& \psi(x,y) = u_\infty R\left(\frac{2\xi}{Re}\right)^{\frac{1}{2}}f(\xi,\eta), \quad u = \frac{\partial\psi}{\partial y}, \quad v = -\frac{\partial\psi}{\partial x}, \quad Re = \left(\frac{\rho u_\infty R}{\mu}\right), \\
& u_\infty = w_\infty\sin(\theta), \quad w = w_e S = w_\infty\cos(\theta)S, \quad G = \frac{T-T_\infty}{T_W-T_\infty}, \quad H = \frac{C-C_\infty}{C_W-C_\infty},
\end{aligned}
\right\} \tag{7}
$$

In view of Equation (7), we have

$$u = 2u_\infty\sin\left(\tfrac{x}{R}\right)F$$

$$v = u_\infty\left\{-\frac{y}{R}\left(2\cos\left(\tfrac{x}{R}\right) - \frac{\sin^2\left(\frac{x}{R}\right)}{(1-\cos\left(\frac{x}{R}\right))}\right)F - \left(\frac{2}{Re\xi}\right)^{\frac{1}{2}}f.\sin\left(\tfrac{x}{R}\right) - \left(\frac{2\xi}{Re}\right)^{\frac{1}{2}}2\sin\left(\tfrac{x}{R}\right)f_\xi\right\}$$

Now, utilizing Equation (7), Equations (2)–(5) are reduced as below, and Equation (1) is satisfied identically.

$$F_{\eta\eta} + fF_\eta + \beta(\xi)\left(1-F^2\right) + 2\xi\left(F_\eta f_\xi - FF_\xi\right) + Ri\,t(\xi)\{(1+\beta_T G)G + (1+\beta_c H)NcH\}\sin(\theta) = 0 \tag{8}$$

$$S_{\eta\eta} + fS_\eta + 2\xi\left(S_\eta f_\xi - FS_\xi\right) + Rip(\xi)\{(1+\beta_T G)G + (1+\beta_c H)NcH\}\sin(\theta) = 0 \tag{9}$$

$$G_{\eta\eta} + PrfG_\eta + 2\xi\left(G_\eta f_\xi - FG_\xi\right)Pr + PrEc\left(4\sin^2(\overline{x})\sin^2(\theta)F_\eta^2 + \cos^2(\theta)S_\eta^2\right) = 0 \tag{10}$$

$$H_{\eta\eta} + ScfH_\eta + 2\xi\left(H_\eta f_\xi - FH_\xi\right)Sc - \Delta p(\xi)ScH^n = 0 \tag{11}$$

The non-dimensional border conditions are given below:

$$
\left.
\begin{aligned}
\text{at } \eta = 0: \quad & F = 0,\ S = 0,\ G = 1,\ H = 1, \\
\text{as } \eta \to \infty, \quad & F = 1,\ S = 1,\ G = 0,\ H = 0
\end{aligned}
\right\} \tag{12}
$$

The dimensionless characteristics employed in the examination are

$$\beta(\xi) = -\frac{\xi\cos\left(\frac{x}{R}\right)}{\sin^2\left(\frac{x}{R}\right)}, \ Ri = \frac{g\beta_T(T_w - T_\infty)R}{u_\infty^2}, \ t(\xi) = \frac{\xi}{4\sin^3\left(\frac{x}{R}\right)}, \ Nc = \frac{\beta_C(C_w - C_\infty)}{\beta_T(T_w - T_\infty)},$$

$$p(\xi) = \frac{\xi}{2 > \sin^2\left(\frac{x}{R}\right)}, \ Ec = \frac{w_\infty^2}{C_p(T_w - T_\infty)}, \ \beta_T = \frac{\beta_2(T_w - T_\infty)}{\beta_1}, \ \beta_C = \frac{\beta_4(C_w - C_\infty)}{\beta_3} \tag{13}$$

Furthermore, $f(\xi, \eta) = \int_0^\eta F d\eta + f_w$, where $f_w = 0$ represents an impermeable wall.
The velocity distribution is

$$u_e(\overline{x}) = 2u_\infty \sin(\overline{x}), \ w_e(\overline{x}) = w_\infty \cos(\theta) = \text{constant, where} \ \overline{x} = \frac{x}{R} \tag{14}$$

Here, ξ, $\beta(\xi)$, $s(\xi)$, and $p(\xi)$ are defined as

$$\xi = 2(1 - \cos(\overline{x})), \ \beta(\overline{x}) = \frac{2\cos(\overline{x})}{(1 + \cos(\overline{x}))},$$

$$s(\overline{x}) = \frac{1}{2\sin(\overline{x})(1 + \cos(\overline{x}))} \ \text{and} \ p(\overline{x}) = \frac{1}{(1 + \cos(\overline{x}))} \tag{15}$$

The expressions $t(\xi)$ and $p(\xi)$ appear in the momentum equations for chordwise and spanwise directions, respectively, containing two variables ξ and $\overline{x}$. In order to reduce into the single variable, we use the following relation, for which the equations are expressed in terms of $\overline{x}$ instead of ξ:

$$\xi\frac{\partial}{\partial\xi} = B(\overline{x})\frac{\partial}{\partial\overline{x}} \tag{16}$$

Here,

$$B(\overline{x}) = \tan\left(\frac{\overline{x}}{2}\right) \tag{17}$$

Using Equations (16) and (17), Equations (8)–(11) reduce as below:

$$F_{\eta\eta} + fF_\eta + 2B(\overline{x})\left(F_\eta f_{\overline{x}} - FF_{\overline{x}}\right) + \beta(\overline{x})\left(1 - F^2\right) +$$
$$+ Ri \cdot t(\overline{x})\{(1 + \beta_T G)G + (1 + \beta_c H)NcH\}\sin(\theta) = 0 \tag{18}$$

$$S_{\eta\eta} + fS_\eta + 2B(\overline{x})\left(S_\eta f_{\overline{x}} - FS_{\overline{x}}\right) + Ri \cdot p(\overline{x})\{(1 + \beta_T G)G + (1 + \beta_c H)NcH\}\sin(\theta) = 0 \tag{19}$$

$$G_{\eta\eta} + PrfG_\eta + 2B(\overline{x})Pr\left(G_\eta f_{\overline{x}} - FG_{\overline{x}}\right) + PrEc\left(4\sin^2(\overline{x})\sin^2(\theta)F_\eta^2 + \cos^2(\theta)S_\eta^2\right) = 0 \tag{20}$$

$$H_{\eta\eta} + ScfH_\eta + 2B(\overline{x})Sc\left(H_\eta f_{\overline{x}} - FH_{\overline{x}}\right) - \Delta p(\overline{x})ScH^n = 0 \tag{21}$$

The relevant boundary constraints are

$$\left.\begin{array}{l} \text{at } \eta = 0: \quad F = 0, \ S = 0, \ G = 1, \ H = 1, \\ \text{as } \eta \to \infty: \quad F = 1, \ S = 1, \ G = 0, \ H = 0 \end{array}\right\} \tag{22}$$

All variables and dimensionless characteristics that take place in the examination and their description are given in Nomenclature.
Drag parameter along the chordwise direction is

$$C_f = \frac{2\left(\mu\frac{\partial u}{\partial y}\right)_w}{\rho w_\infty^2},$$

$$C_f = \frac{2\mu\left(4\frac{u_\infty}{R}\sin^2(\overline{x})\left(\frac{Re}{2\xi}\right)^{0.5}F_\eta(\overline{x},0)\right)\sin^2(\theta)}{\rho u_\infty^2}, \quad (u_\infty = w_\infty\sin(\theta))$$

$$C_f = \frac{4(1+\cos(\overline{x}))(1-\cos(\overline{x}))^{0.5}\sin^2(\theta)F_\eta(\overline{x},0)}{Re^{0.5}}, \tag{23}$$

$$\text{i.e., } Re^{0.5}C_f = 4(1+\cos(\overline{x}))(1-\cos(\overline{x}))^{0.5}\sin^2(\theta)F_\eta(\overline{x},0)$$

Skin-friction coefficient along the spanwise direction is

$$
\overline{C}_f = \frac{2\left(\mu \frac{\partial w}{\partial y}\right)_w}{\rho w_\infty^2},
$$

$$
\overline{C}_f = \frac{2\mu\left(2w_e \frac{\sin(\overline{x})}{R}\left(\frac{Re}{2\zeta}\right)^{0.5} S_\eta(\overline{x},0)\right)\sin^2(\theta)}{\rho u_\infty^2}, \ (w_e = w_\infty \cos(\theta))
$$

$$
\overline{C}_f = \frac{2^{1.5}\cos\left(\frac{\overline{x}}{2}\right)\sin(\theta)\cos(\theta)S_\eta(\overline{x},0)}{Re^{0.5}},
$$

$$
\text{i.e., } Re^{0.5}\overline{C}_f = 2^{1.5}\cos\left(\tfrac{\overline{x}}{2}\right)\sin(\theta)\cos(\theta)S_\eta(\overline{x},0) \tag{24}
$$

Energy transport strength is

$$
Nu = -\frac{R\left(\frac{\partial T}{\partial y}\right)_w}{(T_w - T_\infty)},
$$

$$
Nu = -\frac{R\left((T_w - T_\infty)\frac{2\sin(\overline{x})}{R}\left(\frac{Re}{2\zeta}\right)^{0.5}G_\eta(\overline{x},0)\right)}{(T_w - T_\infty)},
$$

$$
\frac{Nu}{(Re)^{0.5}} = -\left(2\sin(\overline{x})\tfrac{1}{2}\left(\frac{1}{1-\cos(\overline{x})}\right)^{0.5}G_\eta(\overline{x},0)\right),
$$

$$
Re^{-0.5}Nu = -\left(\frac{\sin(\overline{x})}{(1-\cos(\overline{x}))^{0.5}}G_\eta(\overline{x},0)\right),
$$

$$
Re^{-0.5}Nu = -\left(\frac{2\sin\left(\frac{\overline{x}}{2}\right)\cos\left(\frac{\overline{x}}{2}\right)}{2^{0.5}\sin\left(\frac{\overline{x}}{2}\right)}G_\eta(\overline{x},0)\right) \quad \left(\because (1-\cos(\overline{x})) = 2\sin^2\left(\tfrac{\overline{x}}{2}\right)\right)
$$

$$
Re^{-0.5}Nu = -\sqrt{2}\cos\left(\tfrac{\overline{x}}{2}\right)G_\eta(\overline{x},0) \tag{25}
$$

Mass transport strength is

$$
Sh = -\frac{R\left(\frac{\partial C}{\partial y}\right)_w}{(T_w - T_\infty)},
$$

$$
Sh = -\frac{R\left((C_w - C_\infty)\frac{2\sin(\overline{x})}{R}\left(\frac{Re}{2\zeta}\right)^{0.5}H_\eta(\overline{x},0)\right)}{(C_w - C_\infty)},
$$

$$
\frac{Sh}{Re^{0.5}} = -\left(2\sin(\overline{x})\tfrac{1}{2}\left(\frac{1}{1-\cos(\overline{x})}\right)^{0.5}H_\eta(\overline{x},0)\right),
$$

$$
Re^{-0.5}Sh = -\left(\frac{\sin(\overline{x})}{(1-\cos(\overline{x}))^{0.5}}H_\eta(\overline{x},0)\right),
$$

$$
Re^{-0.5}Sh = -\left(\frac{2\sin\left(\frac{\overline{x}}{2}\right)\cos\left(\frac{\overline{x}}{2}\right)}{2^{0.5}\sin\left(\frac{\overline{x}}{2}\right)}H_\eta(\overline{x},0)\right) \quad \left(\because (1-\cos(\overline{x})) = 2\sin^2\left(\tfrac{\overline{x}}{2}\right)\right)
$$

$$
Re^{-0.5}Sh = -\sqrt{2}\cos\left(\tfrac{\overline{x}}{2}\right)H_\eta(\overline{x},0) \tag{26}
$$

3. Solution Technique

Equations (18)–(21) are reduced employing the quasilinearization method as follows:

$$
F_{\eta\eta}{}^{i+1} + A_1^i F_\eta{}^{i+1} + A_2^i F_{\overline{x}}^{i+1} + A_3^i F^{i+1} + A_4^i G^{i+1} + A_5^i H^{i+1} = A_6^i \tag{27}
$$

$$
S_{\eta\eta}{}^{i+1} + B_1^i S_\eta{}^{i+1} + B_2^i S_{\overline{x}}^{i+1} + B_3^i F^{i+1} + B_4^i G^{i+1} + B_5^i H^{i+1} = B_6^i \tag{28}
$$

$$
G_{\eta\eta}{}^{i+1} + C_1^i G_\eta{}^{i+1} + C_2^i G_{\overline{x}}^{i+1} + C_3^i F^{i+1} + C_4^i F_\eta{}^{i+1} + C_5^i S_\eta{}^{i+1} = C_6^i \tag{29}
$$

$$
H_{\eta\eta}{}^{i+1} + D_1^i H_\eta{}^{i+1} + D_2^i H_{\overline{x}}^{i+1} + D_3^i H^{i+1} + D_4^i F^{i+1} = D_5^i \tag{30}
$$

Here, the parameters at the $(i+1)^{th}$ iteration are found using the known i^{th} iteration. The dimensionless border constraints are

$$
\left.\begin{array}{l}
F^{i+1} = 0, \ S^{i+1} = 0, \ G^{i+1} = 1, \ H^{i+1} = 1 \text{ at } \eta = 0 \\
F^{i+1} = 1, \ S^{i+1} = 1, \ G^{i+1} = 0, \ H^{i+1} = 0 \text{ at } \eta = \eta_\infty
\end{array}\right\} \tag{31}
$$

where the border layer limit is η_∞.

Parameters in Equations (27)–(30) are

$$A_1^i = f + 2B(\overline{x})f_{\overline{x}},\, A_3^i = -2B(\overline{x})F,\, A_3^i = -2\beta(\overline{x})F - 2B(\overline{x})F_{\overline{x}},$$
$$A_4^i = Ri \cdot t(\overline{x})(1 + 2\beta_T G)\sin(\theta),\, A_5^i = Ri \cdot t(\overline{x})(1 + 2\beta_C H)Nc \cdot \sin(\theta),$$
$$A_6^i = -2B(\overline{x})FF_{\overline{x}} - \beta(\overline{x})(1 + F^2) + Ri \cdot t(\overline{x})(\beta_T G^2 + Nc\beta_C H^2)\sin(\theta)$$

$$B_1^i = f + 2B(\overline{x})f_{\overline{x}},\, B_2^i = -2B(\overline{x})F,\, B_3^i = -2B(\overline{x})S_{\overline{x}},$$
$$B_4^i = Ri \cdot p(\overline{x})(1 + 2\beta_T G)\sin(\theta),\, B_5^i = Ri \cdot p(\overline{x})(1 + 2\beta_C H)Nc\sin(\theta),$$
$$B_6^i = -2B(\overline{x})FS_{\overline{x}} + Ri \cdot p(\overline{x})(\beta_T G^2 + Nc\beta_C H^2)\sin(\theta)$$

$$C_1^i = Pr(f + 2B(\overline{x})f_{\overline{x}}),\, C_2^i = -2PrB(\overline{x})F,\, C_3^i = -2PrB(\overline{x})G_{\overline{x}},$$
$$C_4^i = -8\sin^2(\overline{x})\sin^2(\theta)PrEcF_\eta,\, C_5^i = -2\cos^2(\theta)PrEcS_\eta,$$
$$C_5^i = 4\sin^2(\overline{x})\sin^2(\theta)PrEcF_\eta^2 + PrEc\cos^2(\theta)S_\eta^2 - 2PrB(\overline{x})G_{\overline{x}}F$$

$$D_1^i = Sc(f + 2B(\overline{x})f_{\overline{x}}),\, D_2^i = -2ScB(\overline{x})F,\, D_3^i = -\Delta Scp(\overline{x})nH^{n-1},\, D_4^i = -2ScB(\overline{x})H_{\overline{x}},$$
$$D_5^i = \Delta Scp(\overline{x})(1-n)H^n - 2ScB(\overline{x})FH_{\overline{x}}$$

The nonlinear coupled partial differential Equations (18)–(21) under the boundary conditions (22) have been solved numerically using an implicit finite difference scheme in combination with the quasilinearization technique. The quasilinearization technique can be viewed as a generalization of the Newton–Raphson approximation method in functional space. An iterative sequence of linear equations is carefully constructed to approximate the nonlinear Equations (18)–(21) under the boundary conditions (22) achieving quadratic convergence and monotonicity and applying the quasilinearization technique, and the nonlinear coupled partial differential Equations (18)–(21) with boundary conditions (22) are replaced by the sequence of linear ordinary differential equations. Since the method is presented for ordinary differential equations by Inouye and Tate [54], and partial differential equations in a recent study by Singh and Roy [55], its detailed description is not provided here. At each iteration step, the sequence of linear partial differential Equations (27)–(30) is expressed in difference form using a central difference scheme in the $\overline{x}$-direction and a backward difference scheme in the η direction. Thus, in each step, the resulting equations have been reduced to a linear algebraic equations system with a block tri-diagonal matrix, which is solved by Varga's algorithm [56]. To ensure the convergence of the numerical solution to the exact solution, step sizes $\Delta\overline{x}$ and $\Delta\eta$ are taken as 0.01 and 0.01. A convergence criterion based on the relative difference between the current and previous iteration values is employed. When the difference reaches 0.0001, the solution is assumed to have converged, and the iteration process is terminated, i.e.,

$$max\left\{\left|(F_\eta)_w^{i+1} - (F_\eta)_w^i\right|,\, \left|(S_\eta)_w^{i+1} - (S_\eta)_w^i\right|,\, \left|(G_\eta)_w^{i+1} - (G_\eta)_w^i\right|,\, \left|(H_\eta)_w^{i+1} - (H_\eta)_w^i\right|\right\} \le 10^{-4}$$

The developed computational code has been validated using data of other authors [18,57]. Thus, comparison of the velocity profiles is made with the steady-state results of Eswara and Nath [57] in the case of $\theta = 0$, $Ec = 0$, and $A = 0$, who studied the problem of an unsteady non-similar two-dimensional and axi-symmetric water boundary layer flow. This comparison presented in Figure 2 illustrates an excellent agreement.
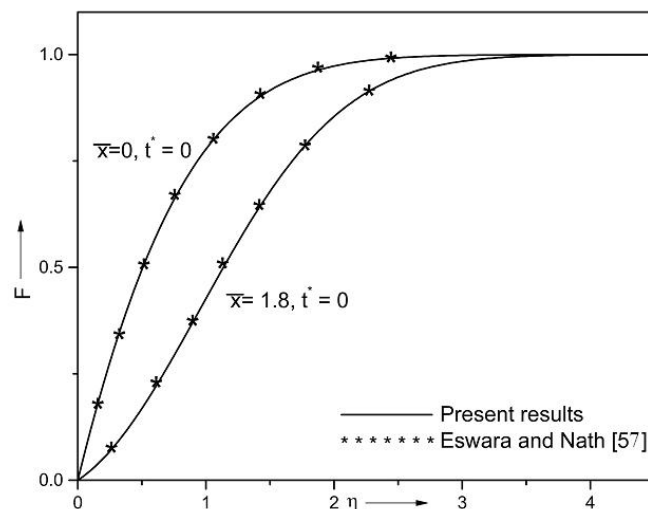
Figure 2. Comparison of velocity profile $F(\overline{x}, \eta)$ with the particular case of flow over cylinder for $\theta = 0$, $Ec = 0$, and $A = 0$.

A comparison of the effect of constant properties on the heat transfer rate is made with the steady-state results of Jenifer et al. [18]. This comparison presented in Figure 3 illustrates an excellent agreement. Table 1 includes comparison of the heat transfer rate for different values of the non-similar variable $(\overline{x})$ and yaw angle (θ) with the data of Jenifer et al. [18].
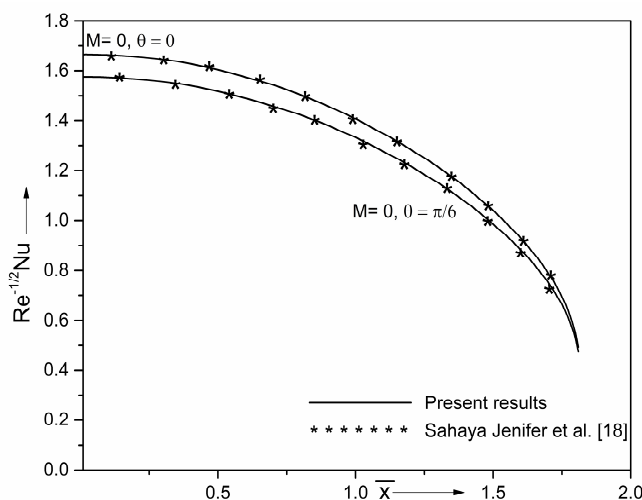

Figure 3. Comparison of the effect of constant properties on the heat transfer rate $\left(Re^{-0.5} Nu \right)$.

Table 1. Comparison of heat transfer rate $\left(Re^{-0.5} Nu \right)$ values of Jenifer et al. [18] for different values of the non-similar variable $(\overline{x})$ and yaw angle (θ).

Non-Similar Variable $(\overline{x})$	Heat Transfer Rate $\left(Re^{-0.5} Nu \right)$			
	Jenifer et al. [18]		Present Results	
	$\theta = 0$	$\theta = \pi/6$	$\theta = 0$	$\theta = \pi/6$
0.01	1.66695	1.57627	1.66696	1.57628
0.2	1.65694	1.56752	1.65694	1.56753
0.5	1.60393	1.51737	1.60394	1.51737
0.7	1.54237	1.4590	1.54238	1.4591
1.0	1.4071	1.33286	1.4072	1.33287

4. Results and Discussion

In order to examine the behavior of the fluid flow over the yawed cylinder, comprehensive computations have been carried out for numerous magnitudes of the non-dimensional characteristics that illustrate the flow, energy, and mass transference and the outcomes are presented graphically. To be more realistic, we have considered water as a host liquid in the investigation and accordingly, $Pr = 7.0$. Moreover, $Sc = 160$ is used for liquid hydrogen. The values of yaw angle (θ), combined convection parameter (Ri), chemical reaction parameter (Δ), Eckert number (Ec), nonlinear temperature convective characteristic (β_T), nonlinear liquid hydrogen concentration convective characteristic (β_C), and the ratio of buoyancy force parameter (Nc) are varied in the ranges $0 \leq \theta \leq \pi/3$, $-1 \leq Ri \leq 10$, $-0.5 \leq \Delta \leq 0.5$, $-0.5 \leq Ec \leq 0.5$, $0 \leq \beta_T \leq 1$, $0 \leq \beta_C \leq 1$, and $0 \leq Nc \leq 1$, respectively. Further, the value $\theta = 0$ represents the perfect vertical wall. The expression $t(\overline{x})$ involved in the buoyancy term of Equation (21) has a singular point exist at $\overline{x} = 0$. However, the boundary exists away from the origin (*i.e.*, $\overline{x} > 0$).

Figures 4 and 5 demonstrate the impact of nonlinear convection coefficient (β_T) and yaw angle (θ) on velocity pattern $F(\overline{x}, \eta)$ and drag coefficient $\left(Re^{0.5} C_f \right)$ in the chordwise direction. Further, the velocity pattern and the drag coefficient increase for increasing magnitudes of the yaw angle. The higher value of the yaw angle (i.e., the cylinder inclines more) characterizes the pressure growth in the liquid flow and increases fluid velocity. The inclination of the cylinder causes the enhancement in the surface friction along the chordwise direction. For the increasing magnitudes of β_T, the velocity patterns and coefficient of friction at the surface increase along the chordwise direction. The larger magnitudes of β_T characterize an essential variation between the cylinder and the environmental temperatures. Therefore, for larger magnitudes of β_T, larger temperature variation reasons strengthen the convection, and as a result, there is the enhancement of the liquid velocity and the friction between the cylinder and liquid. Moreover, we see that the curves obtained by varying the nonlinear convection parameter for zero yaw angle ($\theta = 0$) yield the same results; in fact, these curves overlap into a single curve. This is caused due to both of these parameters appearing together in Equations (18) and (19). Moreover, at $\overline{x} = 1.0$ and $\beta_T = 0.25$, as yaw angle rises between $\theta = \pi/6$ and $\theta = \pi/3$, surface friction coefficient in the chordwise direction increases to about 36%.
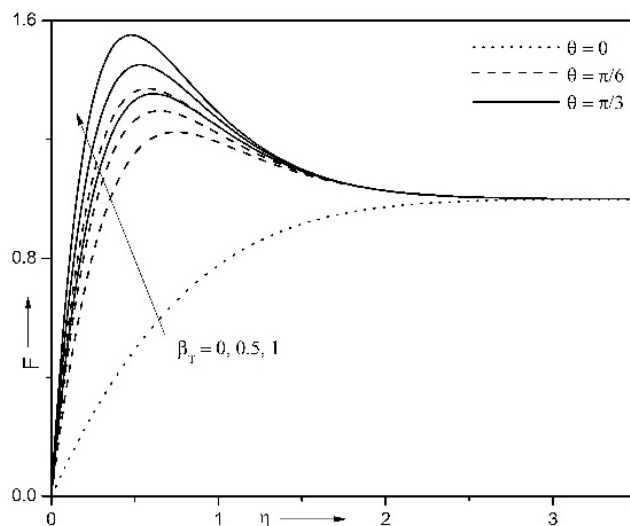

Figure 4. Impact of nonlinear convection characteristic (β_T) and yaw angle (θ) on velocity profile $F(\overline{x}, \eta)$ in the chordwise direction when $\overline{x} = 0.5$, $Pr = 7.0$, $Ri = 10.0$, $\Delta = 0.5$, $Nc = 0.1$, $n = 2$, $Ec = 0.5$, $\beta_C = 0.1$, and $Sc = 160$.
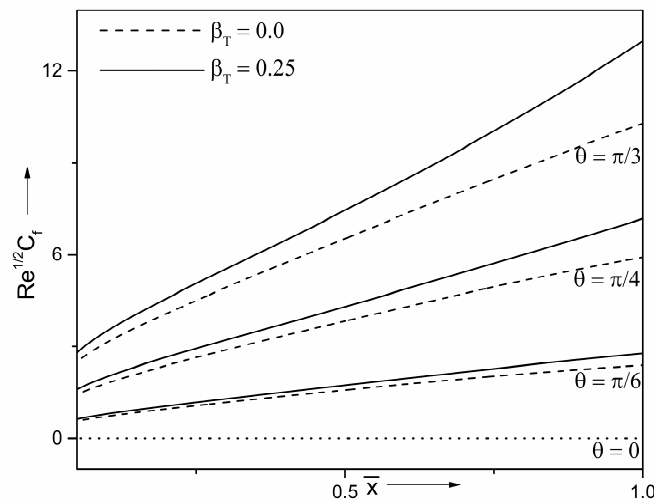
Figure 5. Impact of nonlinear convection characteristic (β_T) and yaw angle (θ) on drag parameter $\left(Re^{0.5}C_f\right)$ in the chordwise direction for $Pr = 7.0$, $Ri = 10$, $\Delta = 0.5$, $Nc = 0.1$, $n = 2$, $Ec = 0.5$, $\beta_C = 0.1$, and $Sc = 160$.

Figures 6 and 7 illustrate the influence of combined convection characteristic (Ri) and yaw angle (θ) on the velocity patterns $S(\overline{x}, \eta)$ and surface drag coefficient $\left(Re^{0.5}\overline{C}_f\right)$ in the spanwise direction. The velocity pattern and drag coefficient rise in the spanwise direction according to the rising magnitudes of the convection parameter. The positive Ri characterizes the significant effect of buoyancy along with the free stream velocity. As a result, the buoyancy within liquid quickens the liquid motion in each direction and concurrently enhances the fluid velocity and respective frictions at the wall. Further, the yaw angle enhances with enhancing magnitudes of the combined convection parameter. Owing to the increase in the inclination of the cylinder, the pressure in the border layer rises within the liquid motion, increasing the liquid velocity in the spanwise direction. The inclination of the cylinder causes an enhancement in the surface friction along the spanwise direction. Furthermore, we observed no variations in the zero yaw angle. However, as yaw angle increases, the friction coefficient in the spanwise direction reduces for opposing buoyancy motion and augments for assisting buoyancy motion.
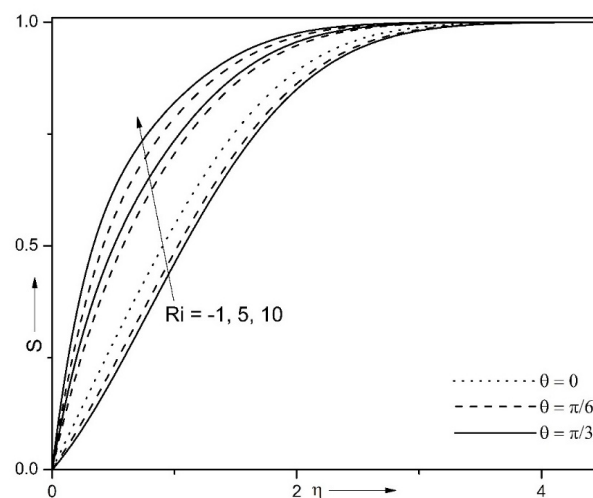

Figure 6. Variation of combined convection characteristic (Ri) and yaw angle (θ) on dimensionless velocity pattern $S(\overline{x}, \eta)$ in the spanwise direction when $\overline{x} = 0.5$, $\beta_T = 0.1$, $Pr = 7.0$, $\Delta = 0.5$, $n = 2$, $Ec = 0.5$, $Nc = 0.1$, $\beta_C = 0.1$, and $Sc = 160$.
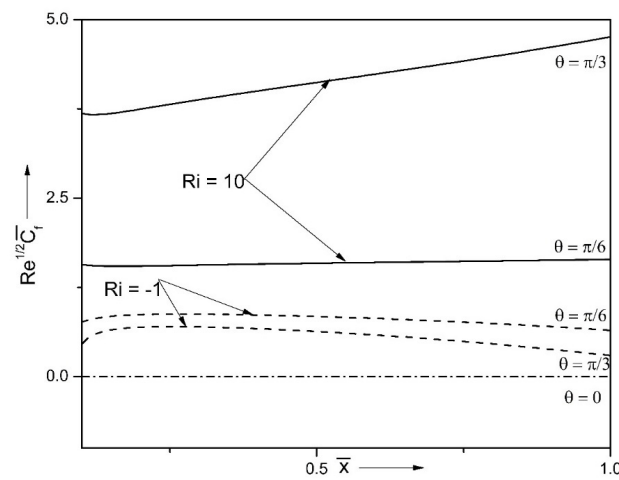
Figure 7. Impact of combined convection characteristic (Ri) and yaw angle (θ) on skin-friction parameter $\left(Re^{0.5}\overline{C}_f\right)$ in the spanwise direction when $Pr = 7.0$, $\beta_T = 0.1$, $\Delta = 0.5$, $Nc = 0.1$, $n = 2$, $Ec = 0.5$, $\beta_C = 0.1$, and $Sc = 160$.

The domination of flow behavior can explain the physical reason in the chordwise direction as θ enhances so that the magnitudes of the skin friction along the spanwise direction decreases. Moreover, at $\overline{x} = 0.5$ and $Ri = 10$, as the inclination angle raises from $\theta = \pi/6$ till $\theta = \pi/3$, the surface friction coefficient is reduced approximately to about 50% in the spanwise direction.

Figures 8 and 9 depict the impact of the Eckert number (Ec) and yaw angle (θ) on the temperature pattern $G(\overline{x}, \eta)$ and energy transference rate $\left(Re^{-0.5}Nu\right)$. The fluid temperature enhances, while the energy transport strength diminishes for the increasing values of Ec. The rising magnitudes of Ec generate more heat owing to the frictional forces among liquid particles that in turn enhance liquid temperature. There is not much impact of the viscous dissipation on the flow characteristics over the yawed cylinder, and these outcomes characterize the reduction rate of heat transfer. Further, the temperature profile diminishes, whereas the rate of energy transference rises for increasing magnitudes of θ.
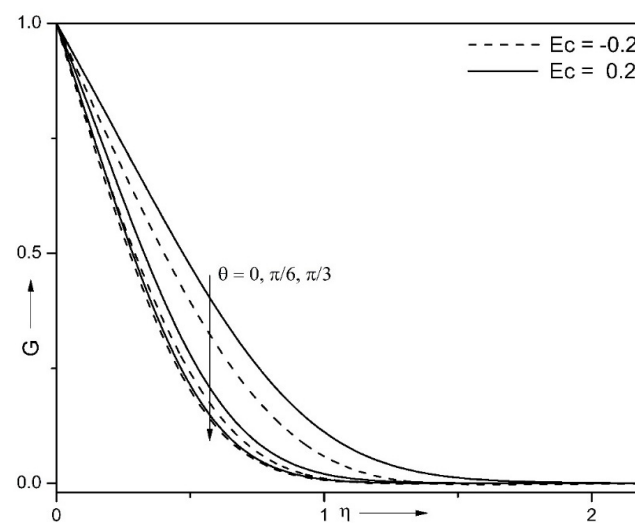

Figure 8. Impact of Eckert number (Ec) and yaw angle (θ) on temperature pattern $G(\overline{x}, \eta)$ when $\overline{x} = 0.5$, $Pr = 7.0$, $\Delta = 0.5$, $Nc = 0.1$, $\beta_T = 0.1$, $Ri = 10$, $n = 2$, $\beta_C = 0.1$, and $Sc = 160$.
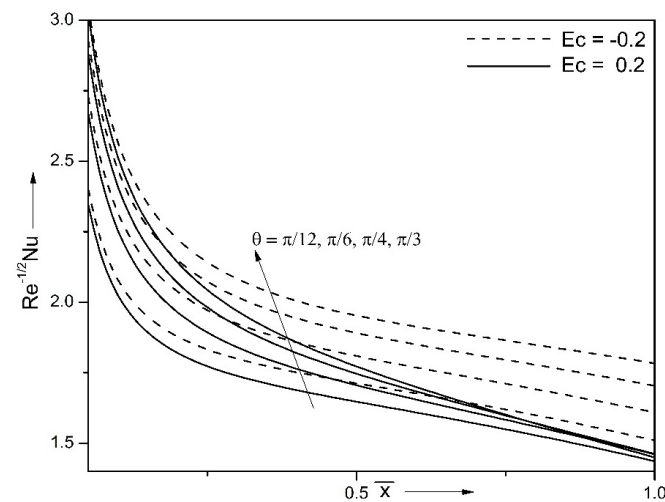
Figure 9. Influence of Eckert number (*Ec*) and yaw angle (θ) on energy transference strength $\left(Re^{-0.5}Nu\right)$ for *Pr* = 7.0, β_T = 0.1, Δ = 0.5, *n* = 2, *Ri* = 10, *Nc* = 0.1, β_C = 0.1, and *Sc* = 160.

Moreover, the liquid temperature diminishes, and the energy transference strength augments, for increasing magnitudes of θ. Furthermore, as the angle changes, the variation has not changed much due to viscous dissipation. With a rise of θ, the medium begins to flow fast, and the temperature reduces, and while high, medium velocity characterizes an opportunity to transport more energy from the shell to the liquid. Moreover, at $\bar{x}$ = 0.5 and *Ec* = −0.1, and as θ increases from π/6 till π/3, the energy transference rate increases approximately 7%. Moreover, at $\bar{x}$ = 0.5 and *Ec* = 0.1, as the inclined angle increases between θ = π/6 and θ = π/3, the Nusselt number increases approximately 5%.

Figures 10–13 demonstrate the impact of the chemical reaction characteristic (Δ), θ, *Sc*, and order of chemical reaction characteristic (*n*) on the non-dimensional concentration pattern $H(\bar{x},\eta)$ and mass transference strength $\left(Re^{-0.5}Sh\right)$. The concentration profile diminishes, and mass transference strength increases as the Schmidt number (*Sc*) increases. This effect explains that the mass diffusivity diminishes for larger values of *Sc*.
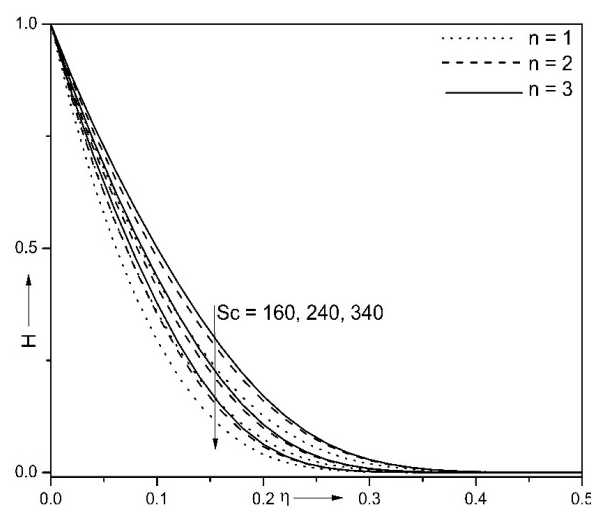

Figure 10. Impact of the order of chemical reaction (*n*) and Schmidt number (*Sc*) on concentration pattern $H(\bar{x},\eta)$ for $\bar{x}$ = 0.5, *Pr* = 7.0, β_T = 0.1, *Ec* = 0.5, *Nc* = 0.1, θ = π/6, *Ri* = 10, β_C = 0.1, and Δ = 0.5.
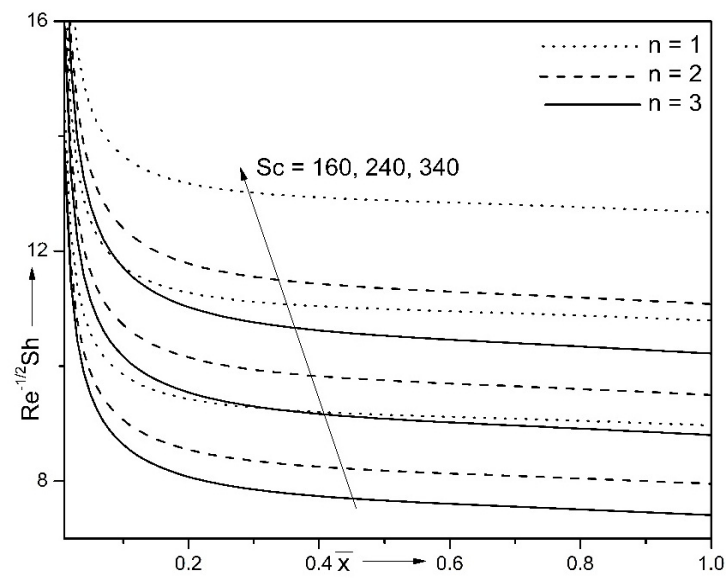
Figure 11. Impact of the order of chemical reaction (*n*) and Schmidt number (*Sc*) on mass transference strength $\left(Re^{-0.5} Sh \right)$ for *Pr* = 7.0, β_T = 0.1, *Ec* = 0.5, *Nc* = 0.1, $\theta = \pi/6$, *Ri* = 10, β_C = 0.1, and Δ = 0.5.

Figure 12. Impact of chemical reaction characteristic (Δ) and yaw angle (θ) on concentration $H(\overline{x}, \eta)$ for $\overline{x} = 0.5$, *Pr* = 7.0, β_T = 0.1, *Ec* = 0.5, *Nc* = 0.1, *n* = 2, *Ri* = 10, β_C = 0.1, and *Sc* = 160.

Figure 13. Influence of chemical reaction parameter (Δ) and yaw angle (θ) on mass transference strength $\left(Re^{-0.5}Sh\right)$ for $Pr = 7.0$, $\beta_T = 0.1$, $Ec = 0.5$, $Nc = 0.1$, $n = 2$, $Ri = 10$, $\beta_C = 0.1$, and $Sc = 160$.
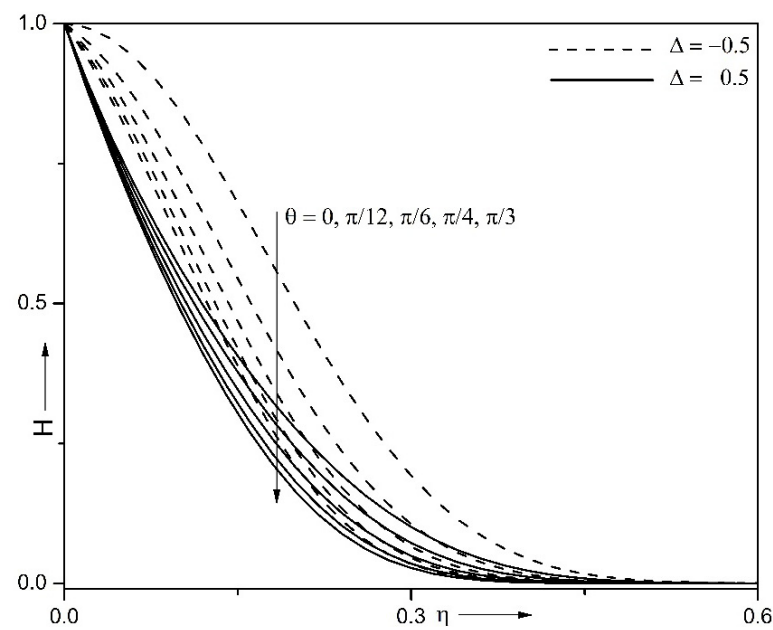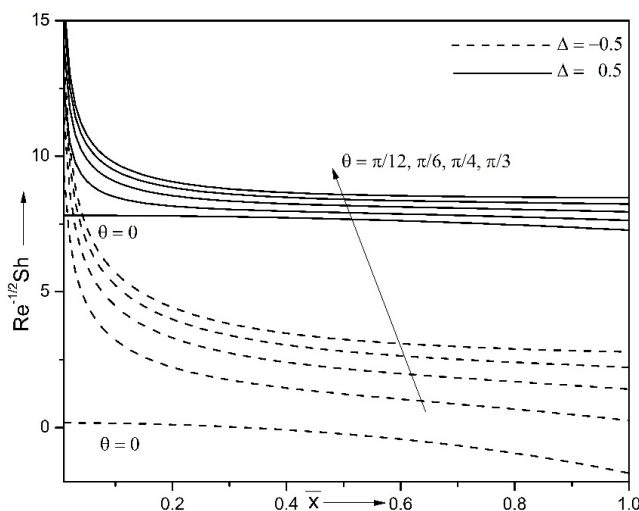
Moreover, the thickness of the concentration border layer reduces as Sc enhances and hence decreases the magnitude of concentration profile; consequently, the Sherwood number increases. It is perceived that for rising values of n, the concentration rises while mass transference strength reduces. The physical reason is that n results in a thickening of the diffusive border layer; therefore, the concentration enhances. Consequently, the Sherwood number reduces. Further, it displays that as the concentration of the liquid decreases while the Sherwood enhances, there is also a rise in the chemical reaction parameter (Δ) and yaw angle (θ). Furthermore, we observe from Figure 11 that the chemical reaction takes place away from the surface significantly. Further, we observe no deviation for $\theta = 0$, representing the vertical cylinder compared to the other yaw angles. In particular, for $\bar{x} = 0.5$ and $n = 2$, the mass transfer rate enhances approximately to 30% as the Schmidt number increases from 160 to 240. Moreover, at $\bar{x} = 0.5$ and $\Delta = 0.5$, as the inclination angle raises between $\theta = \pi/6$ and $\theta = \pi/3$, the Sherwood number increases approximately to about 5%.

Table 2 demonstrates the variations of heat transfer rate for various values of the non-similar variables and the Eckert number. The observation of these values shows that energy transport strength diminishes for the increasing values of the Eckert number. Further, in Table 3, values of the skin-friction coefficient are calculated for different values of the non-similar variable and nonlinear convection parameter. It is observed from Table 3 that the skin friction coefficient increases for the increasing values of the nonlinear convection parameter.

Table 2. Heat transfer rate $\left(Re^{-0.5}Nu\right)$ values for different values of the non-similar variable ($\bar{x}$) and Eckert number (Ec).

Non-Similar Variable ($\bar{x}$)	Heat Transfer Rate $\left(Re^{-0.5}Nu\right)$	
	$Ec = -0.2$	$Ec = 0.2$
0.01	2.72693	2.66956
0.2	2.0366	1.96346
0.5	1.80884	1.70527
0.7	1.72979	1.60646
1.0	1.60905	1.46584

Table 3. Skin-friction coefficient $\left(Re^{0.5}C_f\right)$ values for different values of the non-similar variable $(\bar{x})$ and nonlinear convection (β_T).

Non-Similar Variable ($\bar{x}$)	Skin-Friction Coefficient $\left(Re^{0.5}C_f\right)$	
	$\beta_T = 0.0$	$\beta_T = 0.25$
0.01	0.32626	0.36609
0.2	0.96517	1.05869
0.5	1.58835	1.74631
0.7	1.95581	2.17837
1.0	2.39387	2.76988

Table 4 demonstrates the variations of friction parameter at the surface along the chordwise direction and Nusselt and Sherwood numbers for various magnitudes of yaw angle. From Table 4, it is found that the surface drag coefficient, Nusselt, and Sherwood numbers rise for increasing yaw angles. The friction parameter, strength of heat transference, and mass transport intensity are enhanced by about 80%, 4%, and 7%, respectively, at $\bar{x} = 0.2$, as yaw angle varies from $\pi/12$ to $\pi/6$.

Table 4. Surface drag coefficient along the chordwise direction $\left(Re^{0.5}C_f\right)$, energy transport strength $\left(Re^{-0.5}Nu\right)$, and mass transfer rate $\left(Re^{-0.5}Sh\right)$ values, for the different magnitude of yaw angle ($\theta = 0$ to $\theta = \pi/3$) when $Ri = 10.0$, $\beta_T = 0.1$, $Nc = 0.1$, $n = 2$, $Ec = 0.1$, $\beta_C = 0.1$, $\Delta = 0.1$, and $Sc = 160$.

Yaw Angle (θ)	$\mid Re^{0.5}C_f\mid$	$\mid Re^{-0.5}Nu\mid$	$\mid Re^{-0.5}Sh\mid$
0	0	1.46321	5.74405
$\pi/12$	0.18871	1.50795	6.30997
$\pi/6$	0.99217	1.56392	6.80694
$\pi/3$	4.11030	1.68676	7.37559

5. Conclusions

The performed examination reflects the nonlinear double-diffusive convection circulation over an inclined cylinder under the influence of viscous dissipation and nonlinear chemical reaction. Taking into account the performed investigation, the main conclusions are presented below:

- The temperature profile increases, while heat transport intensity decreases for the growing Eckert number;
- The concentration pattern diminishes for the enhancing nonlinear chemical reaction coefficient;
- For rising magnitudes of the yaw angle, the temperature and concentration profiles diminish, while *Nu* and *Sh* are increased;
- The velocity pattern and drag parameter increase for enhancing magnitudes of the nonlinear convection parameter and yaw angle along the chordwise direction;
- For assisting buoyancy flow, the friction parameter in the spanwise direction enhances for increasing yaw angles.

Thus, the combined consideration of yaw angle, mixed convection, and liquid hydrogen diffusion can significantly enhance and control the flow variations.

Author Contributions: Conceptualization, P.M.P. and H.F.S.; methodology, P.M.P. and H.F.S.; software, H.F.S.; validation, H.F.S.; investigation, P.M.P., H.F.S. and M.A.S.; writing—original draft preparation, P.M.P., H.F.S. and M.A.S.; writing—review and editing, P.M.P., H.F.S. and M.A.S. All authors have read and agreed to the published version of the manuscript.

Nomenclature

C	species concentration;
C_w	species concentration at the border;
C_∞	ambient species concentration;
D_B	Brownian diffusion characteristics ($m^2\,s^{-1}$);
Ec	Eckert number;
F	dimensionless stream function;
g	gravity acceleration ($m\,s^{-2}$);
G	non-dimensional temperature;
Gr	Grashof number;
H	non-dimensional species concentration;
k_1	chemical reaction strength;
n	order of chemical reaction;
Nc	ratio of buoyancy forces characteristic;
Nu	Nusselt number;
Pr	Prandtl number;
R	radius of the cylinder (m);
Ri	mixed convection parameter;
Sc	Schmidt number;
Sh	Sherwood number;
T	temperature (K);
T_w	border temperature (K);
T_∞	environmental temperature (K);
u	velocity projection for the chordwise direction ($m\,s^{-1}$);
u_∞	free stream velocity ($m\,s^{-1}$);
v	velocity projection for the normal direction ($m\,s^{-1}$);
w	velocity projection in the spanwise direction ($m\,s^{-1}$);
x, y and z	curvilinear coordinates(m).

Greek symbols

β_1, β_2	linear and nonlinear heat expansion characteristics, respectively (K^{-1});
β_3, β_4	linear and nonlinear heat expansion characteristics of liquid hydrogen, respectively (K^{-1});
β_C	nonlinear liquid hydrogen concentration convective characteristic;
β_T	nonlinear temperature convective characteristic;
Δ	chemical reaction characteristics;
ψ	stream function ($m^2\,s$);
$\bar{x}$, η	transformed variables;
υ	kinematic viscosity ($m^2\,s^{-1}$);
θ	yaw angle;
$\Delta\bar{x}$, $\Delta\eta$	step sizes for $\bar{x}$ and η coordinates, respectively.

Subscripts

e	indicates the condition at the boundary layer edge;
w	indicates the border condition;
$\bar{x}$, η	define the partial derivatives with respect to these variables;
∞	indicates the condition at the mainstream.

References

1. Revathi, G.; Saikrishnan, P.; Chamkha, A. Non-similar solutions for unsteady flow over a yawed cylinder with non-uniform mass transfer through a slot. *Ain Shams Eng. J.* **2014**, *5*, 1199–1206. [CrossRef]
2. King, R. Vortex excited oscillations of yawed circular cylinders. *J. Fluids Eng.* **1977**, *99*, 495–501. [CrossRef]

3. Chiu, W.S.; Lienhard, J.H. On real fluid flow over yawed circular cylinders. *J. Fluid Eng.* **1967**, *89*, 851–857. [CrossRef]
4. Bucker, D.; Lueptow, R.M. The boundary layer on a slightly yawed cylinder. *Exp. Fluids* **1998**, *25*, 487–490. [CrossRef]
5. Subhashini, S.V.; Takhar, H.S.; Nath, G. Non-uniform multiple slot injection (suction) or wall enthalpy into a compressible flow over a yawed cylinder. *Int. J. Therm. Sci.* **2003**, *42*, 749–757. [CrossRef]
6. Roy, S. Non-uniform mass transfer wall enthalpy into a compressible flow over a yawed cylinder. *Int. J. Heat Mass Transf.* **2001**, *44*, 3017–3024. [CrossRef]
7. Roy, S.; Saikrishnan, P. Non-uniform slot injection (suction) into water boundary layer flow past yawed cylinder. *Int. J. Eng. Sci.* **2004**, *42*, 2147–2157. [CrossRef]
8. Saikrishnan, P. Boundary layer flow over a yawed cylinder with variable viscosity role of non-uniform double slot suction (injection). *Int. J. Numer. Method Heat Fluid Flow* **2012**, *22*, 342–356.
9. Marshall, J.S. Wake dynamics of a yawed cylinder. *J. Fluid Eng.* **2003**, *125*, 97–103. [CrossRef]
10. Najafi, L.; Firat, E.; Akilli, H. Time-averaged near-wake of a yawed cylinder. *Ocean Eng.* **2016**, *113*, 335–349. [CrossRef]
11. Wang, R.; Cheng, S.; Ting, D.K. Effect of yaw angle on flow structure and cross-flow force around a circular cylinder. *Phys. Fluids* **2019**, *31*, 14107. [CrossRef]
12. Lang, H.; Duan, R.Q. Effect of lateral end plate on flow crossing a yawed circular cylinders. *Appl. Sci.* **2019**, *9*, 1590. [CrossRef]
13. Sears, W.R. The boundary layer of yawed cylinders. *J. Aeronautical Sci.* **1948**, *15*, 49–52. [CrossRef]
14. Snarski, S.R. Flow over yawed circular cylinders: Wall pressure spectra and flow regimes. *Phys. Fluids* **2004**, *16*, 344–359. [CrossRef]
15. Zhao, M.; Cheng, L.; Zhou, T. Direct numerical simulation of three-dimensional flow past a yawed circular cylinder of infinite length. *J. Fluids Struct.* **2009**, *25*, 831–847. [CrossRef]
16. Thapa, J.; Zhao, M.; Zhou, T.; Cheng, L. Three-dimensional simulation of vortex shedding flow in the wake of a yawed circular near a plane boundary at a Reynolds number of 500. *Ocean Eng.* **2014**, *87*, 25–39. [CrossRef]
17. Gupta, T.R.; Sarma, G.N. Effect of cross-flow in unsteady flow past a yawed infinite cylinder. *Indian J. Pure Appl. Math.* **1975**, *6*, 1047–1065.
18. Jenifer, A.S.; Saikrishnan, P.; Rajakumar, J. Steady MHD flow over a yawed cylinder with mass transfer. *Front. Heat Mass Transf.* **2021**, *17*, 4. [CrossRef]
19. Khan, U.; Zaib, A.; Ishak, A. Non-similarity solutions of radiative stagnation point flow of a hybrid nanofluid through a yawed cylinder with mixed convection. *Alex. Eng. J.* **2021**, *60*, 5297–5309. [CrossRef]
20. Vajravelu, K.; Sastri, K.S. Fully developed laminar free convection flow between two parallel vertical walls. *Int. J. Heat Mass Transf.* **1977**, *20*, 655–660. [CrossRef]
21. Bhargava, R.; Agarwal, R.S. Fully developed free convection flow in a circular pipe. *Indian J. Pure Appl. Math.* **1979**, *10*, 357–365.
22. Mandal, I.C.; Mukhopadhyay, S. Nonlinear convection in micropolar fluid flow past an exponentially stretching sheet in an exponentially moving stream with thermal radiation. *Mech. Adv. Mater. Struct.* **2018**, *26*, 2040–2046. [CrossRef]
23. Khan, M.I.; Hayat, T.; Waqas, M.; Khan, M.I.; Alsaedi, A. Entropy generation minimization (EGM) in nonlinear mixed convective flow of nanomaterial with Joule heating and slip condition. *J. Mol. Liq.* **2018**, *256*, 108–120. [CrossRef]
24. Tang, J.; Qi, C.; Ding, Z.; Afrand, M.; Ya, Y. Thermo-hydraulic performance of nanofluids in a bionic heat sink. *Int. Commun. Heat Mass Transf.* **2021**, *127*, 105492. [CrossRef]
25. Tu, J.; Qi, C.; Tang, Z.; Tian, Z.; Chen, L. Experimental study on the influence of bionic channel structure and nanofluids on power generation characteristics of waste heat utilisation equipment. *Appl. Therm. Eng.* **2022**, *202*, 117893. [CrossRef]
26. Khan, U.; Zaib, A.; Ishak, A.; Sherif, E.S.M.; Waini, I.; Chu, Y.M.; Pop, I. Radiative mixed convective flow induced by hybrid nanofluid over a porous vertical cylinder in a porous media with irregular heat sink/source. *Case Stud. Therm. Eng.* **2022**, *30*, 101711. [CrossRef]
27. Tu, J.; Qi, C.; Li, K.; Tang, Z. Numerical analysis of flow and heat characteristic around micro-ribbed tube in heat exchanger system. *Powder Technol.* **2022**, *395*, 562–583. [CrossRef]
28. Saha, S.; Hasan, M.N.; Khan, I.A. Double diffusive mixed convection heat transfer inside a vented square cavity. *Chem. Eng. Res. Bull.* **2009**, *13*, 17–24. [CrossRef]
29. Sheremet, M.A.; Pop, I.; Ishak, A. Double-diffusive mixed convection in a porous open cavity filled with a nanofluid using Buongiorno's model. *Transp. Porous Media* **2015**, *109*, 131–145. [CrossRef]
30. Kumar, A.; Singh, R.; Tripathi, R.; Seth, G.S. Double diffusive magnetohydrodynamic natural convection flow of Brinkman type nanofluid with diffusion-thermo and chemical reaction effects. *J. Nanofluids* **2018**, *7*, 338–349. [CrossRef]
31. Grosan, T.; Pop, I. Axisymmetric mixed convection boundary layer flow past a vertical cylinder in a nanofluid. *Int. J. Heat Mass Transf.* **2011**, *54*, 3139–3145. [CrossRef]
32. Prasannakumara, B.C.; Gnaneshwara Reddy, M.; Thammanna, G.T.; Gireesha, B.J. MHD Double-diffusive boundary-layer flow of a Maxwell nanofluid over a bidirectional stretching sheet with Soret and Dufour effects in the presence of radiation. *Nonlinear Eng.* **2018**, *7*, 195–205. [CrossRef]
33. Abdal, S.; Ali, B.; Younus, S.; Ali, L.; Mariam, A. Thermo-Diffusion and multislip effects on MHD mixed convection unsteady flow of micropolar nanofluid over a shrinking/stretching sheet with radiation in the presence of heat source. *Symmetry* **2020**, *12*, 49. [CrossRef]

34. Lund, L.A.; Omar, Z.; Khan, I.; Baleanu, D.; Nisar, K.P. Convective effect on magnetohydrodynamic (MHD) stagnation point flow of Casson fluid over a vertical exponentially stretching/shrinking surface: Triple solutions. *Symmetry* **2020**, *12*, 1238. [CrossRef]

35. Patil, P.M.; Shankar, H.F.; Sheremet, M.A. Mixed convection of silica–molybdenum disulphide/water hybrid nanoliquid over a rough sphere. *Symmetry* **2020**, *13*, 236. [CrossRef]

36. Muthukumaran, C.; Bathrinathan, K. Mathematical modeling of mixed convection boundary layer flows over a stretching sheet with viscous dissipation in presence of suction and injection. *Symmetry* **2020**, *12*, 1754. [CrossRef]

37. Zaib, A.; Khan, U.; Khan, I.; Seikh, A.H.; Sherif, E.M. Entropy generation and dual solutions in mixed convection stagnation point flow of micropolar Ti_6Al_4V nanoparticle along a Riga surface. *Processes* **2020**, *8*, 14. [CrossRef]

38. Khan, U.; Zaib, A.; Mebarek-Oudina, F. Mixed convective magneto flow of SiO_2–MoS_2/$C_2H_6O_2$ hybrid nanoliquids through a vertical stretching/shrinking wedge: Stability analysis. *Arab. J. Sci. Eng.* **2020**, *45*, 9061–9073. [CrossRef]

39. Hsiao, K.-L. To promote radiation electrical MHD activation energy thermal extrusion manufacturing system efficiency by using Carreau-nanofluid with parameters control method. *Energy* **2017**, *130*, 486–499. [CrossRef]

40. Patil, P.M.; Doddagoudar, S.H.; Hiremath, P.S. Impacts of surface roughness on mixed convection nanoliquid flow with liquid hydrogen/nitrogen diffusion. *Int. J. Numer. Method Heat Fluid Flow* **2019**, *29*, 2146–2174. [CrossRef]

41. Patil, P.M.; Roy, S.; Moitsheki, R.J.; Momoniat, E. Double diffusive flows over a stretching sheet of variable thickness with or without surface mass transfer. *Heat Transf.* **2017**, *46*, 1087–1103. [CrossRef]

42. Patil, P.M.; Latha, D.N.; Roy, S.; Momoniat, E. Double diffusive mixed convection flow from a vertical exponentially stretching surface in presence of the viscous dissipation. *Int. J. Heat Mass Transf.* **2017**, *112*, 758–766. [CrossRef]

43. Srinivasacharya, D.; Swamy Reddy, G. Chemical reaction and radiation effects on mixed convection heat and mass transfer over a vertical plate in power-law fluid saturated porous medium. *J. Egypt. Math. Soc.* **2016**, *24*, 108–115. [CrossRef]

44. Kumar, A.; Singh, R.; Tripathi, R.; Seth, G.S. Soret effect on transient magnetohydrodynamic nanofluid flow past a vertical plate through a porous medium with second order chemical reaction and radiation influence. *Int. J. Heat Technol.* **2018**, *36*, 1430–1437. [CrossRef]

45. Malarselvi, A.; Bhuvaneswari, M.; Sivasankaran, S.; Ganga, B.; Abdul Hakeem, A.K. Impacts of chemical reaction on MHD double-diffusive flow with suction/blowing and slip. *J. Phys. Conf. Ser.* **2018**, *1139*, 12089. [CrossRef]

46. Patil, P.M.; Latha, D.N.; Roy, S.; Momoniat, E. Non-similar solutions of mixed convection flow from an exponentially stretching surface. *Ain Shams Eng. J.* **2017**, *6*, 55. [CrossRef]

47. Patil, P.M.; Chamkha, A.J. Heat and mass transfer from mixed convection flow of polar fluid along a plate in porous media with chemical reaction. *Int. J. Numer. Method Heat Fluid Flow* **2013**, *23*, 899–926. [CrossRef]

48. Hayat, T.; Rashid, M.; Alsaedi, A.; Asghar, S. Nonlinear convective flow of Maxwell nanofluid past a stretching cylinder with thermal radiation and chemical reaction. *J. Braz. Soc. Mech. Sci. Eng.* **2019**, *41*, 86. [CrossRef]

49. Reddy, P.S.; Chamkha, A. Heat and mass transfer analysis in natural convection flow of nanofluid over a vertical cone with chemical reaction. *Int. J. Numer. Method Heat Fluid Flow* **2017**, *27*, 2–22. [CrossRef]

50. Schlichting, H.; Gersten, K. *Boundary Layer Theory*; Springer: New York, NY, USA, 2000.

51. Patil, P.M.; Shashikant, A.; Roy, S.; Hiremath, P.S. Mixed convection flow past a yawed cylinder. *Int. Commun. Heat Mass Transf.* **2020**, *114*, 104582. [CrossRef]

52. Patil, P.M.; Roy, S. Corrigendum of "Mixed convection flow past a yawed cylinder" [ICHMT 114 (2020) 104582]. *Int. Commun. Heat Mass Transf.* **2021**, *124*, 105246. [CrossRef]

53. Patil, P.M.; Shankar, H.F.; Sheremet, M.A. Nonlinear mixed convective flow over a moving yawed cylinder driven by buoyancy. *Mathematics* **2021**, *9*, 1275. [CrossRef]

54. Inouye, K.; Tate, A. Finite difference version Quasilinearization applied to boundary layer equations. *AIAA J.* **1974**, *12*, 558–560. [CrossRef]

55. Singh, P.J.; Roy, S. Unsteady mixed convection from a rotating vertical slender cylinder in an axial flow. *Int. J. Heat Mass Transf.* **2008**, *51*, 1423–1430. [CrossRef]

56. Verga, R.S. *Matrix Iterative Analysis*; Prentice-Hall: Englewood Cliffs, NJ, USA, 2000.

57. Eswara, E.T.; Nath, G. Unsteady non-similar two-dimensional and axisymmetric water boundary layers with viscosity and Prandtl number. *Int. J. Eng. Sci.* **1994**, *32*, 267–279. [CrossRef]